Phase Behavior and Viscoelastic Properties of Thermoplastic Elastomer Gels Based on ABC Triblock Copolymers

Daisuke Yamaguchi,*,†,§ Michel Cloitre,† Pierre Panine,‡ and Ludwik Leibler†

Laboratoire Matière Molle et Chimie (UMR ESPCI-CNRS 7167), ESPCI, 10 rue Vauquelin, 75231 Paris Cedex 05, France, and European Synchrotron Radiation Facility, BP 220, 38043 Grenoble Cedex, France

Received February 9, 2005; Revised Manuscript Received July 5, 2005

ABSTRACT: The structure and the rheological properties of thermoplastic elastomer gels composed of polystyrene-*block*-polybutadiene-*block*-poly(methyl methacrylate) triblock copolymer (SBM) in a selective solvent for the midblock have been investigated over a wide range of concentrations. At low polymer concentration, the S and M endblocks are mixed into spherical microdomains and SBM gels behave like ordinary ABA triblocks. At sufficiently large polymer concentration, S and M are segregated in distinct cylindrical or lamellar microdomains dispersed in an elastomer matrix comprising the B midblocks swollen with the solvent. The low-frequency storage modulus significantly increases upon demixing. Hence, under appropriate conditions, the presence of two different endblocks in ABC copolymers can promote bridge formation and lead to elastomer gels with improved mechanical performance.

I. Introduction

ABA block copolymers composed of hard endblocks and soft midblocks constitute an important class of thermoplastic elastomers.[1] In many cases, the endblocks are styrenic blocks (S) while the midblocks are saturated (EB) or unsaturated (B, I) diene blocks. When dissolved in a midblock selective solvent, ABA copolymers associate to form micellar solutions at low concentration[2] and physical gels at large concentration.[3] In gels, the endblocks form spherical, cylindrical, or lamellar microdomains depending on the incompatibility between A and B, on the block lengths, and on the polymer concentration.[4] ABA thermoplastic gels display several interesting rheological features, in particular when the glass transition temperature of the A endblocks is larger than that of the B midblocks.[5−12] At temperatures below T_g^A and above T_g^B, the network formed by the B blocks exhibits a rubbery behavior while the A blocks form glassy domains. Above T_g^A but below the order−disorder transition temperature, the A chains can be pulled out under large deformation, yielding plastic flow. Above the order−disorder temperature, solutions behave much like ordinary viscoelastic liquids.

A particular attention has been paid to the conformation of the rubbery midblocks.[13] Indeed, ABA copolymers are tethered at both ends, yielding two different possible conformations for the midblocks: (i) loops when both endblocks belong to the same microdomain; (ii) bridges when the endblocks connect two different microdomains. It has been shown that loops and bridges bring different contributions to the elasticity and that any change in the loop/bridge populations affects the low-frequency storage modulus of the gels.[14−16] In addition, if the entanglement length is significantly smaller than the length of the midblocks, there exist entanglements between bridges and loops, which also contribute to the elasticity of the gels.[5,17]

The objective of this paper is to analyze the difference of behavior between thermoplastic gels made from ABA and ABC block copolymers. The ABC copolymers considered in the following are polystyrene (S)−polybutadiene (B)−poly(methyl methacrylate) (M) designated as SBM hereafter. SBM block copolymers, and their mixtures with SB diblocks and with homopolymers, have been found to exhibit a wealth of morphologies[18−25] and to offer promising routes toward high-performance nanostructured materials.[26] One potential advantage of SBM copolymers over their ABA counterparts (like SBS) is that the midblocks B have necessarily a bridge conformation when the endblocks A and C belong to different microdomains. Brinkmann-Rengel et al. followed this line of thought in their attempt to design SBM thermoplastic elastomers with improved elastic properties.[27] In most instances, they found no major difference between the behavior of SBM and that of SBS. The main reason invoked was that the S and M blocks were only slightly incompatible, yielding mixed S and M glassy microdomains, which was detrimental for the bridge population.

In this paper, we investigate thermoplastic elastomer gels made of SBM triblock copolymers in a selective solvent for the midblock. The addition of a selective solvent brings additional degree of freedom and offers interesting opportunities to tune at the same time the morphology, the phase behavior of the S and M endblocks, and the bridge population. The evolution of the rheological behavior with the solvent concentration is particularly interesting in that respect. At low polymer concentration, the S and M endblocks form mixed microdomains and SBM behave like ordinary ABA triblocks. At sufficiently large polymer concentration, S and M are segregated in distinct glassy microdomains dispersed in an elastomer matrix comprising the B midblocks swollen with oil. The material remains a gel up to the glass temperature transition of the M blocks. The demixing of S and M is associated with a large

† UMR ESPCI-CNRS 7167.
‡ European Synchrotron Radiation Facility.
§ Present address: Soft Matter Neutron Scattering Research Group, Advanced Science Research Center, Japan Atomic Energy Research Institute, Tokai-mura, Ibaraki 319-1195, Japan.
* Corresponding author. E-mail: daisukey@neutrons.tokai.jaeri.go.jp.

10.1021/ma050294e CCC: $30.25
Published on Web 08/13/2005

Table 1. Properties of SBM Block Copolymers and Oil Used in the Experiments

component	M_n (kg/mol)[a]	wt %[b]	f[c]	ρ (g/cm^3)[d]	ρ_e (e/nm^3)[e]
S	17	0.25	0.27	1.049	340
B	28	0.41	0.44	0.892	298
M	23	0.34	0.29	1.188	386
oil				0.76	261

[a] M_n(S) is determined by GPC; M_n(B) and M_n(M) are calculated from the composition. [b] Weight fraction of blocks determined from ^{1}H NMR. [c] Volume fractions of blocks calculated from the weight fractions and the densities ρ. [d] Densities taken from ref 47. [e] Electronic densities calculated from the chemical composition and the densities.

increase of the low-frequency storage modulus, yielding improved rheological behavior.

II. Experimental Part

II.1. Materials. In the following, we study a polystyrene (S)−polybutadiene (B)−poly(methyl methacrylate) (M) triblock copolymer synthesized and provided by Arkema.[28] The average molecular mass is about 68 kg/mol. The products issued from the synthesis contain a certain amount of SB diblock copolymer identical to the SB part in SBM (ca. 20 wt %) and a small amount of polystyrene homopolymer (ca. 3 wt %). The SB diblocks were extracted by circulation of *n*-heptane at 90 °C for 48 h. The selectivity and the efficiency of the extraction were checked by ^{1}H NMR and size exclusion chromatography (SEC). The experimental method is presented in ref 29. The final product obtained after purification contains less than 1 wt % of SB diblock and will be considered as pure SBM. The polydispersity index is PDI ≅ 1.4. In a previous work we analyzed the origin of the polydispersity in SBM block copolymers, which were synthesized in the same conditions. The polydispersity of the S and M blocks was studied by SEC after selective ozonolysis of the B block. We found that the S and M blocks had the same polydispersity index (PDI ≅ 1.2), resulting in a total polydispersity index of about 1.4. The presence of polystyrene (ca. 4 wt %) was considered to have no effect on the phase behavior of the gels. The characteristics of the purified SBM copolymer used in the experiments are shown in Table 1.

Blends were obtained by mixing SBM copolymers with an aliphatic oil that is a selective solvent for the B midblock (Plastol 355 commercially available from Esso). This oil has a low vapor pressure, and no discernible evaporation was detected even when the samples were kept several hours at high temperature.

II.2. Sample Preparation. The solutions were prepared by dissolving the desired amount of copolymer and antioxidant (Irganox, Ciba-Geigy Group) (2 wt %) in chloroform before adding the prescribed amount of oil. Chloroform, which is a good solvent of SBM copolymers, acts as a cosolvent, allowing fast and efficient dissolution. The solutions were subsequently cast in Petri dishes for quiescent solvent removal at ambient temperature over 1 week. Then the samples were heated at 80 °C under vacuum for 24 h to evaporate the residual solvent. The resulting specimens are designated hereafter as "non-annealed". For each blend composition, we also prepared "annealed" specimens by keeping "nonannealed" specimens at a temperature of 180 °C (e.g., well above the glass transition temperature of poly(methyl methacrylate)) under vacuum for 12 h. We determined systematically the composition of the annealed samples by ^{1}H NMR measurements and checked that no degradation had occurred during annealing, within the experimental accuracy. In the following, we study SBM/oil blends in the range 0.10 g/g ≤ C ≤ 0.70 g/g in increments of 0.10 g/g. The polymer concentration C is expressed in g/g.

II.3. Viscoelastic Measurements. Rheological measurements were conducted on a conventional rheometer (C < 0.50 g/g) and a dynamic mechanical analyzer (C ≥ 0.50 g/g). The rheometer was a strain-controlled apparatus (ARES from Rheometrics) equipped with parallel plates (diameter: 25 mm; sample thickness: 1.5−2.5 mm). During heating, gels increase their volume, and we allowed slight variations of the gap distance to maintain the normal force negligible. To identify the linear viscoelastic regime, we first performed dynamic strain sweeps at a frequency of 1 Hz and at different temperatures. When the strain amplitude was in the range 0.005 ≤ γ_0 ≤ 0.03, the stress response was linear in strain over the entire temperature range. Linear viscoelastic measurements showed that, for C ≥ 0.05 g/g, SBM/oil solutions have a solidlike behavior, with the elastic shear modulus $G'(\omega)$ exhibiting a low-frequency plateau much greater than the loss modulus $G''(\omega)$. To determine the temperature properties of the SBM/oil blends, we also performed temperature sweep at a frequency of 1 Hz and measured the storage and loss moduli, G' and G''. The temperature was varied between 5 and 200 °C at a rate of 5 °C/min.

The viscoelastic properties of the most concentrated samples were measured using a dynamic mechanical analyzer (DMA 2980, TA Instruments). The samples were shaped into parallelepipeds (1 × 5 × 20 mm). The tensile storage and loss moduli, E' and E'', were measured at a frequency of 1 Hz between −100 and 180 °C with a rate of 5 °C/min. The relation $E' = 3G'$ was used to relate the tensile storage modulus E' measured by DMA and the shear modulus G' determined by shear rheology. For C = 0.5 g/g both methods can be applied and give similar results within the experimental accuracy.

II.4. Small-Angle X-ray Scattering (SAXS). SAXS measurements were conducted at the high-brilliance beamline (ID-2) of the ESRF (European Synchrotron Radiation Facility, Grenoble, France). The optics was used at a fixed wavelength of λ = 0.1 nm, and sample−detector distance was set at 10 m. The scattering intensity I was obtained as a function of the scattering wave vector magnitude $q = 4\pi\lambda^{-1}\sin(\theta/2)$ where θ is the scattering angle. The data were collected by a Thomson X-ray image intensifier optically coupled to a CCD-based Frelon detector. The spatial resolution is Δq = 0.0075 nm^{-1}. The 2d spectra are averaged over circular domains and normalized to absolute intensities as described in ref 30. The specimens were heated and cooled in a hot stage (Mettler FT82HT) inserted in the beamline, allowing us to probe the structure in real time between 20 and 200 °C, the heating rate being +5 °C/min.

II.5. Transmission Electron Microscopy (TEM). In some cases (C = 0.50 g/g), we conducted TEM observations. Although the blends contain a considerable amount of oil, they have enough rigidity at low temperature to be microtomed. Ultrathin sections of ca. 60 nm thickness were obtained by microtoming at −100 °C using a Reichert-Jung, Ultracut E instrument together with a cryogenic unit FC4E and a diamond knife. The ultrathin sections were picked up on copper grids and then stained by exposure to osmium tetraoxide (OsO_4) vapor for 30 min or ruthenium tetraoxide (RuO_4) vapor for 10 s. TEM observations were performed with a LEO 902 transmission microscope equipped with an imaging camera unit Megaview 2, SIS. In the case of staining with OsO_4, the S phase appears gray on the TEM micrograph, the B phase is dark, and the M phase is white. When stained with RuO_4, the S phase appears dark, the B phase is gray, and the M phase is white.

III. Results

III.1. Mixing of S and M Endblocks. The existence of gel phases where the endblocks S and M are mixed is one of the characteristic features of the SBM/oil blends. This is shown in Figure 1 where we have represented the temperature dependence of the storage modulus G' (E') and loss tangent tan $\delta = G''/G'$ (tan $\delta = E''/E'$) measured by shear rheology and DMA.

The results for pure copolymer show three distinct glass transition temperatures, indicating that the three blocks S, B, and M are segregated into different microdomains. The lowest glass transition temperature is

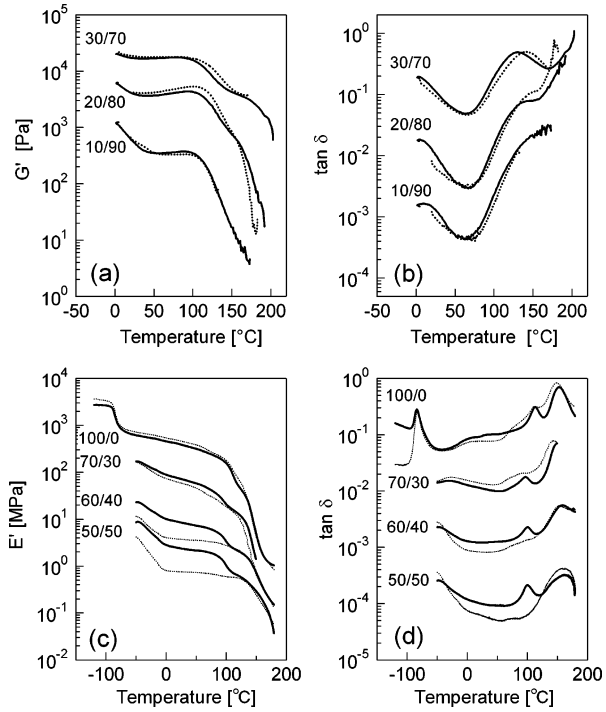

Figure 1. (a, b) Storage modulus (G') and tan(δ) measured by shear rheology as a function of temperature for SBM/oil gels at different polymer concentrations: $C = 0.10$ g/g (10/90), $C = 0.20$ g/g (20/80), $C = 0.30$ g/g (30/70). The tan(δ) data for 20/80 and 10/90 are shifted downward by 1 and 2 decades, respectively, for clarity. (c, d) Young modulus (E') and tan(δ) measured by DMA as a function of temperature for SBM/oil gels at different polymer concentrations: $C = 0.50$ g/g (50/50), $C = 0.60$ g/g (60/40), $C = 0.70$ g/g (70/30), and neat copolymer (100/0). The tan(δ) data for 70/30, 60/40, and 50/50 are shifted downward by 1, 2, and 3 decades, respectively, for clarity. Solid and dotted lines represent the modulus of annealed samples and nonannealed samples, respectively.

that of the B block ($T_g^B \cong -84$ °C). The glass temperature at about 105 °C is that of the S block ($T_g^S \cong 105$ °C). The largest glass transition temperature is that of the M block ($T_g^M \cong 135$ °C). It is interesting to note that the curves before and after annealing are qualitatively the same, indicating that the structure does not change significantly upon annealing. The DMA curves of the most concentrated gels ($C = 0.7$ g/g) have a similar shape. The low-temperature region is not accessible because the oil freezes at about −50 °C, but the two peaks in tan δ at high temperature clearly indicate the glass transition temperatures of the glassy S and M blocks. In the presence of oil, the glass transition temperature associated with the S block is slightly lower ($T_g^{S/oil} \cong 100$ °C) than the glass transition temperature measured in the neat copolymer ($T_g^S \cong 105$ °C), suggesting that a small fraction of oil is dissolved in the S domains at high temperature and acts as a plasticizer.

The results obtained at low polymer concentration ($C \leq 0.3$ g/g) show a completely different behavior. The two well-defined peaks in tan δ associated with the glass transition temperatures of the S and M blocks are replaced by a single broad peak with a maximum located between $T_g^{S/oil}$ and T_g^M. This shows that the glassy microdomains consist of S and M blocks mixed together. The variations of the storage modulus and of the loss tangent do not change upon annealing, indicating that the S and M blocks remain mixed at high temperature.

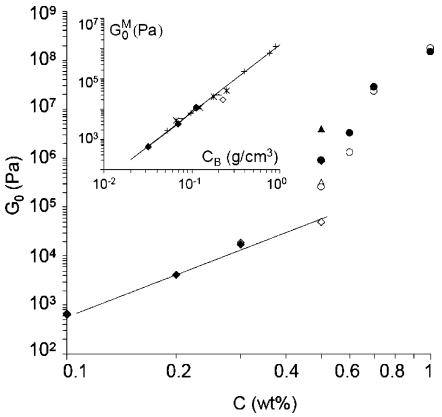

Figure 2. Variations of the low-frequency storage modulus of as-cast (open symbols) and annealed (full symbols) gels as a function of the polymer concentration. For $C < 0.50$ g/g, G_0 is measured directly by shear rheology. For $C \geq 0.50$ g/g, G_0 is deduced from the Young modulus measured by DMA using the relation $E_0 = 3G_0$. The solid line shows that the storage modulus follows a power-law variation for $C < 0.50$ g/g. All data are measured at 20 °C and at a frequency of 1 Hz. For $C = 0.5$ g/g, we use different symbols to distinguish the data obtained in different experiments. The inset shows the variations of the storage modulus of the B matrix as a function of the monomer concentration. The data are compared to the variations of the elastic modulus of linear polybutadiene solutions[41] (+) and to the storage modulus of the B matrix in SBS/tetradecane thermoplastic gels[5] (∗). The slope of the solid line is 2.25.

At intermediate polymer concentration, the S and M blocks are mixed in the as-cast samples, but they demix into different microdomains upon annealing. This is shown in Figure 1 for the two concentrations $C = 0.5$ g/g and $C = 0.6$ g/g. The loss tangent of the as-cast samples exhibits only one broad peak, indicating that the S and M blocks are mixed. After annealing, the loss tangent curves exhibit two peaks corresponding to the glass transitions of the S and M blocks.

III.2. Elastic Properties of SBM/Oil Gels. As is evident from Figure 1, the elastic modulus increases when the oil fraction is decreased. To quantify this observation, the plateau shear modulus G_0 at 20 °C is represented as a function of the polymer weight fraction C in Figure 2. In practice, G_0 is very well approximated by the value of the elastic modulus measured at 1 Hz. At low concentrations ($C \leq 0.5$ g/g), we obtain G_0 directly from the viscoelastic measurements with the ARES rheometer. At large concentration ($C \geq 0.5$ g/g), we perform DMA measurements, and we use the relation $E_0 = 3G_0$ to relate the plateau tensile modulus E_0 to the plateau shear modulus G_0. Figure 2 shows that G_0 increases by several orders of magnitude when C is increased from 0.1 to 0.7 g/g. We also observe that, upon annealing, G_0 is not changed when the polymer concentration is small ($C \leq 0.3$ g/g) or large ($C \geq 0.7$ g/g) while it increases by nearly 1 order of magnitude at intermediate concentration ($C = 0.5$ g/g and $C = 0.6$ g/g).

The increase of the elastic modulus upon annealing at intermediate concentration is associated with a change of the elastic properties of the gels at large deformation. This is shown in Figure 3 where we have represented the stress−strain curves of nonannealed (as-cast) and annealed gels at intermediate concentrations. In these experiments, the samples are subjected to an oscillatory shear strain; the frequency is kept constant (1 Hz), and the amplitude increases steadily. The elastic behavior of as-cast samples is strain-

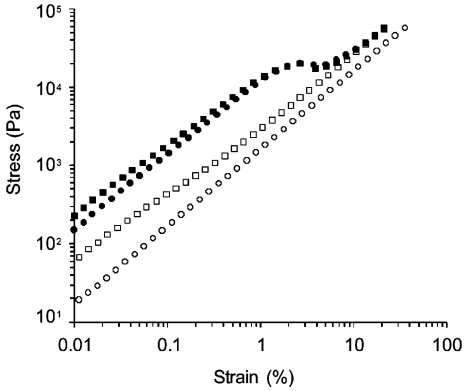

Figure 3. Nonlinear mechanical behavior of a SBM/oil gel at intermediate concentration (C = 0.5 g/g). The stress−strain curves are obtained by shearing the gel between two parallel plates at a constant frequency f = 1 Hz using the ARES rheometer. The different symbols refer to the following successive treatments: ○, as-cast gel before annealing; ●, annealed gel; □, annealed gel after large strain deformation; ■, healed gel after second annealing.

independent up to very large strains (∼100%). By contrast, annealed samples exhibit a surprisingly small linear viscoelastic regime. A sharp yield point is observed at γ_0 = 1%. After yielding, a linear elastic behavior is still observed, but the shear modulus is drastically reduced to a value close to that for nonannealed samples. Interestingly, after removal of the shear stress and a second annealing, the gels heal and recover their initial properties.

III.3. Structure of SBM/Oil Gels. Gels at Low Polymer Concentration. To elucidate the structure of SBM/oil gels, we have performed SAXS experiments. Figure 4 shows the SAXS patterns of a gel in the nonannealed and annealed states when the polymer concentration is low (C = 0.30 g/g). The main effect of annealing is to enhance the intensity of the higher-order scattering peaks. Their positions remain essentially constant, apart from slight shifts that can be associated with local rearrangements leading to an enhancement of the long-range order. The scattering peaks of annealed gels are situated at q values of 1, $\sqrt{2}$, $\sqrt{3}$, $\sqrt{4}$, $\sqrt{5}$, $\sqrt{6}$, and $\sqrt{7}$ relative to the first-order peak position q_m. These are the lattice scattering peaks of spherical microdomains arranged in a cubic symmetry. The value of q_m (q_m = 0.167 nm^{-1}) gives access to the Bragg spacing of the lattice, d_m = 38 nm. In view of the results of the previous section, the spherical microdomains consist of mixed S and M chains. The B midblocks swollen with oil form the continuous phase.

In Figure 4, the intensity of the interference peaks is modulated by a low-frequency function due to intradomain scattering. This modulation is revealed in particular by the deep minima situated at $q \cong 0.3$ nm^{-1}, $q \cong 0.5$ nm^{-1}, and $q \cong 0.7$ nm^{-1}. In practice, the intensity scattered by a spherical microdomain, the so-called form factor, is given by

$$I(q) = I_e V^2(\rho_e^{SM} - \rho_e^{m})^2[f(qR)]^2$$

$$f(qR) = \frac{3}{(qR)^3}[\sin(qR) - (qR)\cos(qR)] \qquad (1)$$

I_e is the intensity scattered by an electron. V is the volume of a spherical microdomain, and R is its radius. ρ_e^{SM} and ρ_e^{m} are the electron densities of a microdomain

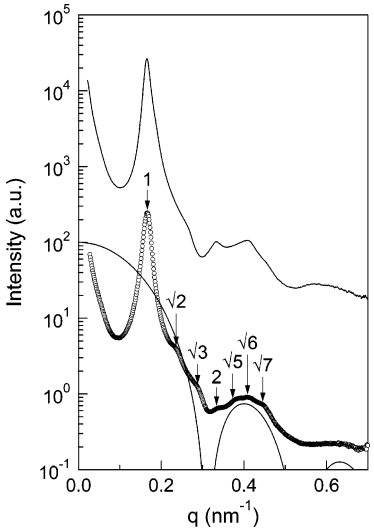

Figure 4. Semilogarithmic plot of the scattered intensity as a function of the scattering vector q for a SBM/oil gel prepared at C = 0.30 g/g, before (−) and after annealing (○). The scattering profile of the annealed gel is shifted downward by 2 decades for clarity. The arrows denote the position of the scattering peaks due to interdomain interference. The thick solid line shows the form factor due to spherical microdomains comprising mixed S and M endblocks (R = 14 nm).

and of the continuous phase, which are estimated directly from the electron densities and the volume fractions of S, B, M, and oil (Table 1). The radius R of the microdomains can be determined by plotting the form factor given by eq 1 for different values of R and selecting for R the value which best reproduces the minima at $q \cong 0.3$ nm^{-1}, $q \cong 0.5$ nm^{-1}, and $q \cong 0.7$ nm^{-1}. Figure 4 shows that the agreement is reasonably good for R = 14 nm.

From the values of d_m and R, it is possible to determine the volume fractions of the mixed S + M spherical microdomains using simple geometrical arguments. For a simple cubic (sc) lattice, the volume fraction should be equal to 0.23; for a body-centered-cubic (bcc) lattice, it should be of the order of 0.16. These values have to be compared with the actual volume fraction deduced from the composition, which is about 0.134 (see Table 2). This comparison shows that the S + M spherical microdomains are arranged in a bcc structure. This result is consistent with the presence of a peak at $\sqrt{7}q_m$ in the SAXS profile, which crucially discriminates a bcc structure from a sc structure.

Annealed Gels at Intermediate Polymer Concentration. Figure 5 presents the scattering profiles of nonannealed and annealed gels at intermediate concentration (C = 0.50 g/g). Now the position and the intensity of the interference peaks change dramatically during annealing, indicating that the structure is completely modified. Let us first analyze the structure of annealed gels. The scattering profile exhibits a first-order peak at q_m = 0.093 nm^{-1}, yielding a long period d_m = 68 nm. The maxima of the higher-order interference peaks are situated at $\sqrt{3}q_m$ and $\sqrt{7}q_m$. There also exists a broad maximum at about $\sqrt{12}q_m$ and/or $\sqrt{13}q_m$. These are the characteristic positions of the scattering peaks of a hexagonal lattice.

We have also performed TEM observations of the gels. Figure 6a presents TEM micrographs of an ultrathin section of gel that has been stained with RuO_4. Staining with RuO_4 reveals preferentially the M blocks that

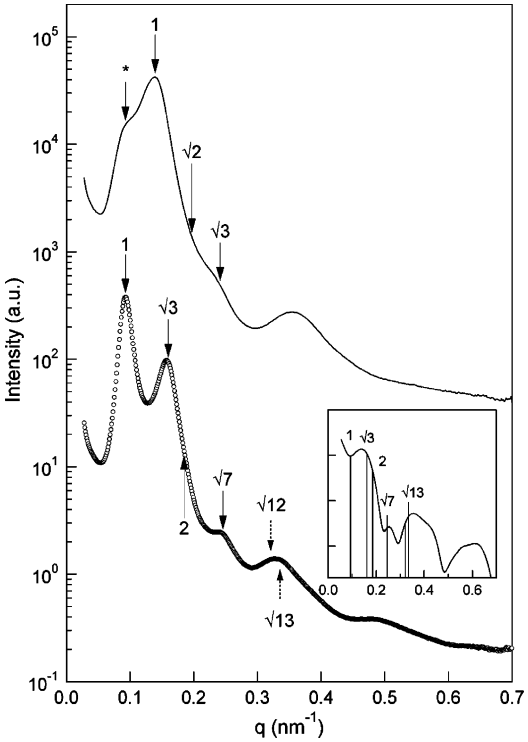

Figure 5. Semilogarithmic plot of the scattered intensity as a function of the scattering vector q for a SBM/oil gel prepared at $C = 0.50$ g/g before (—) and after annealing (○). The scattering profile of the annealed gel is shifted downward by 2 decades for clarity. The arrows denote the position of the scattering peaks due to interdomain interference (the dashed arrows indicate the positions of the peaks expected at $q = \sqrt{12}q_m$ and $q = \sqrt{13}q_m$). The inset shows the scattering profile of the twinned hexagonal structure calculated from the structure factor of an hexagonal lattice and the form factor given by expression 2. The continuous line represents the variations of the form factor. The vertical bars give the intensity of the interference peaks. Only the peaks assigned in the experimental spectrum are represented.

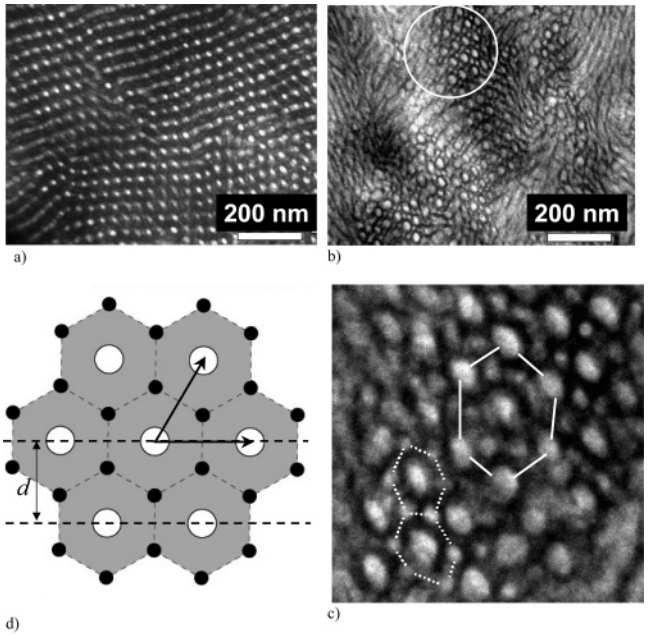

Figure 6. Transmission electron micrographs of an annealed SBM/oil gel at $C = 0.50$ g/g: (a) gel stained with RuO_4; (b) gel stained with OsO_4; (c) zoom of the interior of the circle shown in micrograph (b); the full lines join the centers of six PMMA cylinders forming an hexagon; the dotted lines join the centers of PS cylinders forming hexagons; (d) schematic representation of the twinned hexagonal morphology.

appears white. The white spots with 6-fold symmetry that are visible in Figure 6a are the signature of an hexagonal array of cylinders of M endblocks that have been cut perpendicularly to their long axis. Figure 6b,c presents TEM micrographs of an ultrathin section that has been stained with OsO_4. Staining with OsO_4 causes the B blocks to appear dark in the TEM micrographs whereas the S blocks appear gray and the M blocks appear white. We now distinguish spots and stripes in a continuous dark gray matrix. This observation can be rationalized by considering that the gels consist of cylinders of S and M dispersed in a B matrix. The stripes correspond to cylinders that have been cut along their long axis while the spots reveal the cylinders that have been cut perpendicularly to their long axis. There are two types of cylinders: large white cylinders and small cylinders with a low contrast. The distance between the large cylinders in Figure 6b is the same as that measured in Figure 6a. This allows us to identify unambiguously both families of cylinders: large cylinders comprise the M endblocks while the small ones consist of the S endblocks. The enlargement presented in Figure 6c shows that the small S cylinders are arranged around the M cylinders with a 6-fold symmetry. This leads us to propose the twinned hexagonal structure shown in Figure 6d. S and M blocks form separate cylindrical microdomains arranged in hexagonal order. Each cylinder of M blocks is surrounded by six cylinders of S blocks. The elementary cell is formed by one thick M cylinder and two thin S cylinders.

To confirm this interpretation, it would interesting to compare the SAXS pattern of the twinned hexagonal structure with the experimental spectrum shown in Figure 5. The entire modeling is beyond the scope of this paper, but it is straightforward to calculate the intensity scattered by a twinned hexagonal structure when the direction of the long axis of the cylinders is parallel to the beam. The structure factor is that of an hexagonal lattice.[31] The expression of the form factor is

$$I(q) = I_e\left\{(\rho_e^M - \rho_e^m)f_M(qR_M) + \frac{2(\rho_e^S - \rho_e^m)f_S(qR_S)}{3} \times \left[2\cos\left(\frac{\sqrt{3}}{3}q_x d\right)\cos\left(\frac{1}{3}q_y d\right) + \cos\left(\frac{2}{3}q_y d\right)\right]\right\}^2$$

$$f_i(qR_i) = 2\pi R_i \frac{J_1(qR_i)}{q} \qquad (2)$$

where I_e is the intensity scattered by an electron, and R_M and R_S are the radius of the M and S cylinders, which can be estimated from the volume fractions of the different components: $R_M = 14$ nm and $R_S = 10$ nm. d is the shortest distance between two planes containing M cylinders. J_1 is the Bessel function of the first kind. ρ_e^i and ρ_e^m are the electron densities of the i component and of the matrix phase (i.e., the mixture of B midblocks and oil), respectively. q_x and q_y are the projection of wavevector q along the horizontal and vertical directions. The cylinders are assumed to be of unit length. Using the expressions of the structure factor and of the form factor, we can compute easily the 2d scattering pattern of the twinned hexagonal structure. Averaging

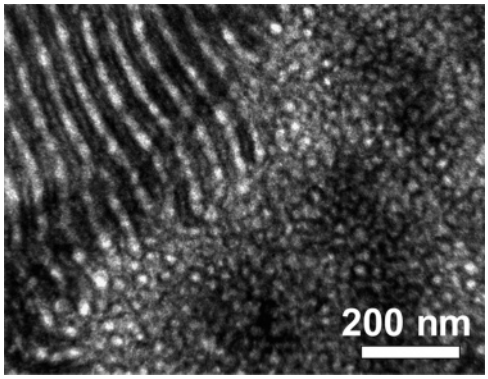

Figure 7. Transmission electron micrographs of a nonannealed SBM/oil gel stained with OsO_4 at $C = 0.50$ g/g.

the intensity over circles of radius q yields the SAXS pattern shown in the inset of Figure 5. The agreement with the experimental spectrum is fairly good given the fact that there is no adjustable parameter. One of the characteristic features present in both the experimental and the calculated spectra, which discriminates the twinned hexagonal structure from a regular hexagonal structure, is the high intensity of the second reflection. This was first noticed in ref 23. In conclusion, the existence of the twinned hexagonal structure we propose is supported by both real and reciprocal space analysis.

Nonannealed Gels at Intermediate Polymer Concentrations. The scattering pattern of a nonannealed gel at intermediate concentration is shown in Figure 5 ($C = 0.5$ g/g). It exhibits a well-defined interference peak at $q_m = 0.148$ nm^{-1}, i.e., nearly at the same position as the first-order interference peak of the gels prepared at low concentrations. At low wave vectors, we also note the presence of a shoulder centered at $q_m = 0.095$ nm^{-1}, which is the position of the first-order interference peak of the annealed gels. This result shows that the nonannealed gels consist of spherical domains of mixed S and M blocks coexisting with cylinders of S and M in a PB/oil matrix. Unfortunately, the higher-order peaks are not sufficiently well-defined to be assigned precisely. To draw a definite conclusion, we have performed TEM observations of the nonannealed gels. A typical micrograph is shown in Figure 7. In the image, the lower right-hand side region seems to show spherical microdomains in a dark matrix of PB/oil, while the upper left-hand side region can be interpreted as a cut of the twinned hexagonal structure shown in Figure 6d by a plane parallel to the long axis of the cylinders. In conclusion, two structures coexist in nonannealed gels at intermediate concentrations: the body-centered-cubic structure typical of the gels at low concentration and the twinned hexagonal structure observed after annealing. It is likely that the relative importance of one structure with respect to the other depends on the conditions of preparation (temperature, kinetics of evaporation, concentration of cosolvent), expressing the fact that nonannealed gels are out-of-equilibrium.

Gels at Large Polymer Concentration. Figure 8 shows the scattering pattern of a gel before and after annealing when the polymer concentration is high ($C = 0.70$ g/g). Upon annealing, the number of Bragg peaks increases and their sharpness is enhanced, but their position is not shifted, indicating that the gel structure is preserved. The positions of the higher-order scattering maxima are integer multiples of the first-order peak position q_m ($q_m = 0.077$ nm^{-1}). This shows that the gels have a lamellar structure with a long period $d_m = 82$ nm.

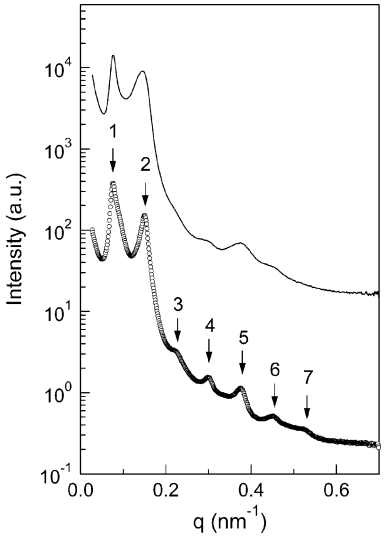

Figure 8. Semilogarithmic plot of the scattered intensity as a function of the scattering vector q for a SBM/oil gel at $C = 0.70$ g/g before (—) and after annealing (○) at 180 °C. The scattering profile of the annealed gel is shifted downward by 2 decades for clarity. The arrows denote the position of the scattering peaks due to lamellar interdomain interference.

Table 2. Volume Fractions of Oil (Φ_{oil}) and SBM Block Copolymer (Φ_{SBM}) at Different Polymer Concentrations and the Effective Volume Fractions of the Different Blocks (f_i')

C (g/g)	Φ_{oil}	Φ_{SBM}	f_S'	f_B'	f_M'
0.3	0.76	0.24	0.07	0.86	0.07
0.5	0.57	0.43	0.12	0.76	0.12
0.7	0.36	0.64	0.17	0.55	0.28

IV. Discussion

IV.1. Morphologies of SBM/Oil Gels. The morphology of SBM/oil gels changes from spheres on a bcc cubic lattice to lamellar morphology through cylinders on a twinned hexagonal lattice when the oil content is decreased. This evolution of the curvature can be rationalized by considering that the role of the selective oil is to swell preferentially the PB midblocks, thereby changing the effective volume fraction of the different blocks.[32] In Table 2, we give the effective volume fractions of the three blocks when the oil content is varied, assuming that the oil is completely selective for the PB matrix phase. Let us start from the neat triblock without solvent. It is nearly symmetric ($f_S = 0.27$, $f_B = 0.44$, $f_M = 0.30$) and forms a lamellar morphology. This structure is preserved as long as the effective volume fraction of the B block swollen with oil remains sufficiently low to ensure that the interfaces between S and B, on one hand, and between S and M, on the other hand, are not curved. At larger oil content, this condition is not fulfilled, interfaces become curved, and the gel structure evolves to a cylindrical morphology. For $C = 0.5$ g/g, the effective volume fraction of the S and M endblocks is equal to 0.24, which is a reasonable value to observe cylindrical morphology in AB and ABA copolymers.[33,34] At this point, it is interesting to note that the twinned hexagonal morphology proposed in Figure 6 has already been observed in SBM copolymers with a slightly different composition:[23] $f_S = 0.21$, $f_B =$

0.62, $f = 0.17$. The morphology was observed in films cast from a benzene−cyclohexane (30:70 wt %) mixture. Since cyclohexane is slightly selective for the B block, it is likely that the effective volume of the B block in solution was higher than expected from the composition, yielding a twinned hexagonal morphology ($f_B' = 0.76$ in our experiments) that was subsequently trapped during evaporation. For $C = 0.3$ g/g, the effective volume fraction of the B block further increases, that of S and M decreases, and the structure evolves to a spherical morphology.

IV.2. Mixing and Demixing of S and M Endblocks. Morphologies where S and M blocks are mixed have already been observed in SBM[27,35]and MSBSM[36] block copolymers. Here we find that, at equilibrium, the S and M endblocks can form a mixed phase or can be fully segregated depending on the polymer concentration. To rationalize our observations, it is useful to follow the approach developed in ref 37. One driving force for the mixing of S and M is the gain of mixing entropy of the junctions between S (or M) and B midblock. Indeed, when S and M are phase-separated, the S/B and M/B junctions are located on different interfaces in a regular order. On the contrary, when S and M are mixed, they can be located randomly on the same interface. The corresponding gain of mixing entropy is

$$\Delta S = -\frac{f_S}{f_S + f_M}\ln\left(\frac{f_S}{f_S + f_M}\right) - \frac{f_M}{f_S + f_M}\ln\left(\frac{f_M}{f_S + f_M}\right) \quad (3)$$

f_S and f_M are the volume fractions of the S and M blocks. The enthalpy penalty associated with the mixing of S and M can be estimated from the expression

$$\Delta H = \chi_{SM} f_S f_M (N_S + N_M) \quad (4)$$

where χ_{SM} is the interaction parameter between S and M. In the following, we take[38] $\chi_{SM} = 0.028 + 3.9/T$ ($\chi_{SM} = 0.037$ at 180 °C). N_S and N_M are the degree of polymerization of blocks S and M. For the symmetric SBM block copolymers studied here, we have $f_S = f_M = (1 - f_B)/2$, and expressions 3 and 4 reduce to

$$\Delta S = \ln(2) \quad \text{and} \quad \Delta H = \chi_{SM}(1 - f_B)^2(N_S + N_M) \quad (5)$$

with $N_S + N_M \cong 400$. Equating these two terms, we find that mixing of S and M is possible ($\Delta S > \Delta H$) when the volume fraction of the midblock B satisfies to $f_B \geq 0.7$.

This result can be used directly to analyze the phase behavior of the S and M blocks. In the absence of solvent, the volume fraction of the midblock being $f_B \cong 0.44$ (Table 1), we predict that the endblocks must be phase-segregated just as observed experimentally. In gels, we apply the same line of thought with the proviso that f_B is now the effective volume fraction f_B'. From Table 2, we deduce that the S and M blocks should form distinct phases when $C = 0.7$ g/g but should be mixed for $C = 0.3$ g/g just as observed experimentally. For $C = 0.5$ g/g, the effective volume fraction f_B' is fairly close to the volume fraction above which mixing is expected; a more accurate analysis would be useful to reproduce the observed experimental behavior.

It is important to note that the mixing and demixing of S and M endblocks in SBM block copolymers are subtle phenomena that may be affected by the protocol of preparation. Here, we start from a solution of SBM and oil in chloroform, which plays the role of a cosolvent. During evaporation, microphase separation takes place in a concentrated solution. Chloroform, which is a good solvent of S and M, reduces the repulsive interactions between the endblocks and promotes mixing. At some point, the structure does not evolve just because some of the components have become glassy. In that respect, the morphology of as-cast samples may represent a quenched structure that is not representative of the structure at thermodynamic equilibrium. This explains in particular why, at intermediate concentration, the S and M endblocks are mixed in as-cast samples and segregated in annealed samples.

IV.3. Elastic Modulus of Gels with Mixed Endblocks. When the endblocks are mixed, Figure 2 shows that the plateau storage modulus G_0 is a power law function of the polymer concentration: $G_0 \sim C^{\beta}$. This nonlinear dependence suggests that the "flower" model proposed by Semenov et al.[17] applies here. This model considers that midblocks form loops and bridges and that the topological constraints due to loop and bridge entanglements control the gel elasticity. In SBM/oil gels, the existence of midblock entanglements is supported by the fact that the molecular weight between entanglements of polybutadiene is fairly low[39] ($M_e^B = 1900$ g/mol). In view of this, it is tempting to make an analogy between SBM/oil gels and cross-linked polymer rubbers reinforced with glassy spherical fillers.[5,40] We then express the shear storage modulus, G_0, as a function of the shear modulus of the B matrix, G_0^M, using the following expression:

$$G_0 = (1 + 2.5\Phi_g + 14.1\Phi_g^{\,2})G_0^M \quad (6)$$

where Φ_g is the volume fraction of the glassy spherical inclusions. For G_0^M, we take the storage modulus of an entangled nonassociating polybutadiene solution in the semidilute regime:

$$G_0^M \sim C_B^{\,9/4} \quad (7)$$

where C_B is the polybutadiene concentration in the matrix. Inserting G_0^M given by (7) into expression 6, we obtain a prediction of the storage modulus of SBM/oil gels as a function of the polymer concentration. It is not convenient to compare directly this prediction with the experimental data because the volume fraction of glassy phase is itself a function of the polymer concentration. We prefer to correct the modulus from the reinforcement effect and to plot $G_0^M = G_0/(1 + 2.5\Phi_g + 14.1\Phi_g^2)$ versus the polymer concentration in the matrix, C_B. The result is shown in the inset of Figure 2. For $C \leq 0.3$ g/g and for the as-cast gel prepared at $C = 0.50$ g/g, the data representing G_0^M versus C_B in a double-logarithmic scale fall on a straight line, in agreement with the scaling law in expression 7. It is interesting to note that the values of G_0^M deduced from our experiments are very close to the values of the storage modulus of linear polybutadiene solutions[41] and to similar data measured for SBS/*n*-tetradecane gels.[5] This shows that the elastic modulus of SBM/oil gels at low concentration is dominated by the existence of entanglements between the B midblocks.

IV.4. Change of Elastic Properties during Annealing (Intermediate Concentration). Figures 2 and 3 show that the storage modulus of SBM/oil gels increases by at least 1 order of magnitude upon anneal-

ing and that annealed gels exhibit a plastic-to-rubber transition at large deformation. In the following we interpret these observations taking into account the cylindrical morphology of the annealed samples and the demixing of the glassy endblocks into distinct microdomains.

In the literature, there are several comprehensive studies of the deformation behavior of SBS block copolymers in macroscopically oriented specimens with cylindrical morphologies.[42−44] It has been shown that the mechanical response is highly anisotropic depending on the orientation of the glassy microdomains with respect to direction of deformation. When the microdomains are oriented along the deformation, the sample behaves like a simple mechanical model of two phases connected in parallel. The storage modulus is large because the glassy microdomains with the highest elastic modulus transmit most of the stress. Plastic flow is reached at very small deformations. Above the yield point, the rigid cylinders are fragmented into smaller pieces that simply play the role of discontinuous filler particles reinforcing the matrix. Samples with cylinders perpendicular to the deformation respond like a series connection of the different phases. The elastic modulus is close to that of the rubbery matrix. Plastic failure still occurs but at a much higher deformation. In both cases, upon annealing, the original structure heals and the original mechanical properties are recovered.

In the absence of any special treatment, samples are not macroscopically oriented. Orientational order is restricted to small regions with a size of some microns. Inside a grain, cylinders have a preferential orientation. Adjacent grains have different orientations so that the distribution of orientations in a macroscopic sample can be considered as isotropic. As for the mechanical properties, thermoplastic gels composed of SEPS and SIS copolymers in a midblock selective solvent do not exhibit any particular increase of the storage modulus when the morphology changes from spherical to cylindrical (apart from a trivial concentration effect).[11] SBS samples also exhibit a conventional mechanical behavior although plastic-to-rubber transitions have been reported in some cases.[45,46]

By contrast, the mechanical behavior of annealed SBM/oil gels is that of microcomposites where the cylinders are connected and form a rigid network. The change of mechanical properties during annealing (and demixing of the S and M blocks) can be interpreted as a transition from a state in which the glassy endblocks behave as discontinuous rigid fillers in a rubbery matrix to a state where they are connected and transmit most the stress. However, when the deformation is large enough, the cylinders become fragmented and again they behave as discontinuous fillers.

To explain this behavior, we take into account different factors. First, the formation of a rigid percolating network must depend critically on the number density of cylinders in the matrix. In that respect, the situation where the endblocks are segregated in distinct microdomains is highly favorable because the number density of cylinders is twice that in a simple hexagonal morphology with mixed endblocks. The number and the type of defects between adjacent grains are other important factors. It is likely that the configuration where the midblocks form bridges connecting the glassy cylinders promotes continuity between grains. Bridges have another important role: they transmit efficiently most of the mechanical forces between neighboring rigid cylinders. This can explain why the gels yields at relatively low deformation.

This description suggests that the mechanical properties must be very sensitive to the bridge population and therefore to the degree of demixing. This is particularly important since the mechanism leading to the separation of S and M is strongly dependent on the initial state and since long-lived defects can remain trapped in the annealed samples.[36] This can explain the dispersion of the values of the storage modulus values both in as-cast and annealed gels.

V. Concluding Comments

This work shows that the mechanical properties of SBM/oil thermoplastic elastomer gels share features with those of ABA and ABC block copolymers. At low polymer concentrations, the S and M endblocks are mixed and form spherical microdomains in a B matrix. The rheological properties are dominated by the entanglements of the midblocks in the matrix. At larger polymer concentration, S and M are segregated in distinct glassy microdomains of cylindrical morphology. The storage modulus increases by at least 1 order of magnitude due the formation a continuous network of glassy microdomains that transmits the stress. This occurs for a relatively low volume fraction of glass phase ($\cong$0.24), in contrast to what is observed in ABA block copolymers.

Acknowledgment. D.Y. gratefully acknowledges support from ATOFINA (now ARKEMA) and Total through a postdoctoral fellowship. The authors thank Arkema for providing the block copolymer samples used in this study and in particular Drs F. Court and C. Navarro. We are grateful to P. Coupard for his help during the TEM experiments. The authors are indebted to Dr. T. Narayanan for providing access to the ID02 beamline and for his help during the experiments. D.Y. is indebted to Professor H. Watanabe for an enlightening discussion.

References and Notes

(1) See for example: *Thermoplastic Elastomers−A Comprehensive Review*; Holden, G., Kricheldorf, H. R., Quirk, R. P., Eds.; Hanser Publishers: Munich, Germany, 2004.
(2) Hamley, I. W. *The Physics of Block Copolymers*; Oxford University Press: Oxford, 1998; Chapter 3.
(3) Hamley, I. W. *The Physics of Block Copolymers*; Oxford University Press: Oxford, 1998; Chapter 4.
(4) Spontak, R. J.; Patel, N. P. *Curr. Opin. Colloid Interface Sci.* **2000**, *5*, 334−341.
(5) Watanabe, H.; Kuwahara, S.; Kotaka, T. *J. Rheol.* **1984**, *28*, 393−409.
(6) Raspaud, E.; Lairez, D.; Adam, M.; Carton, J. P. *Macromolecules* **1996**, *29*, 1269−1277.
(7) Sato, T.; Watanabe, H.; Osaki, K. *Macromolecules* **1996**, *29*, 6231−6239.
(8) Laurer, J. H.; Mulling, J. F.; Khan, S. A.; Spontak, R. J.; Bukovnik, R. *J. Polym. Sci., Part B: Polym. Phys.* **1998**, *36*, 2379−2391.
(9) Laurer, J. H.; Mulling, J. F.; Khan, S. A.; Spontak, R. J.; Lin, J. S.; Bukovnik, R. *J. Polym. Sci., Part B: Polym. Phys.* **1998**, *36*, 2513−2523.
(10) King, M. R.; White, S. A.; Smith, S. D.; Spontak, R. J. *Langmuir* **1999**, *15*, 7886−7889.
(11) Laurer, J. H.; Khan, S. A.; Spontak, R. J.; Satkowski, M. M.; Grothaus, J. T.; Smith, R. J.; Lin, J. S. *Langmuir* **1999**, *15*, 7947−7955.
(12) Vega, D. A.; Sebastian, J. M.; Loo, Y. L.; Register, R. A. *J. Polym. Sci., Part B: Polym. Phys.* **2001**, *39*, 2183-2197.

(13) Watanabe, H. *Macromolecules* **1995**, *28*, 5006−5011.
(14) Watanabe, H.; Sato, T.; Osaki, K.; Yao, M. L.; Yamagishi, A. *Macromolecules* **1997**, *30*, 5877−5892.
(15) Watanabe, H.; Sato, T.; Osaki, K. *Macromolecules* **2000**, *33*, 1686−1691.
(16) Watanabe, H.; Sato, T.; Osaki, K. *Macromolecules* **2000**, *33*, 2545−2550.
(17) Semenov, A. N.; Joanny, J.-F.; Khokhlov, A. R. *Macromolecules* **1995**, *28*, 1066−1075.
(18) Auschra, C.; Stadler, R. *Macromolecules* **1993**, *26*, 2171−2174.
(19) Zheng, W.; Wang, Z. G. *Macromolecules* **1995**, *28*, 7215−7223.
(20) Stadler, R.; Auschra, C.; Beckmann, J.; Krappe, U.; Voigt-Martin, I.; Leibler, L. *Macromolecules* **1995**, *28*, 3080−3091.
(21) Krappe, U.; Stadler, R.; Voigt-Martin, I. *Macromolecules* **1995**, *28*, 4558−4561.
(22) Breiner, U.; Krappe, U.; Thomas, E. L.; Stadler, R. *Macromolecules* **1998**, *31*, 135−141.
(23) Brinkmann, S.; Stadler, R.; Thomas, E. L. *Macromolecules* **1998**, *31*, 6566−6572.
(24) Goldacker, T.; Abetz, V. *Macromolecules* **1999**, *32*, 5165−5167.
(25) Goldacker, T.; Abetz, V.; Stadler, R.; Erukhimovich, I. Ya.; Leibler, L. *Nature (London)* **1999**, *398*, 137−139.
(26) Ritzenthaler, S.; Court, F.; David, L.; Girard-Reydet, E.; Leibler, L.; Pascault, J. P. *Macromolecules* **2002**, *35*, 6245−6254. Ritzenthaler, S.; Court, F.; Girard-Reydet, E.; Leibler, L.; Pascault, J. P. *Macromolecules* **2003**, *36*, 118−123.
(27) Brinkmann-Rengel, S.; Abetz, V.; Stadler, R.; Thomas, E. L. *Kautsch. Gummi Kunstst.* **1999**, *12*, 806−813.
(28) Navarro, C.; Marcarian, X.; Vuillemin, B. *Macromol. Symp.* **1998**, *132*, 263−269.
(29) Fleury, C. Doctoral Thesis, Université Pierre et Marie Curie, 2001.
(30) Narayanan, T.; Diat, O.; Boesecke, P. *Nucl. Instrum. Methods Phys. Res.* **2001**, *A467−468,*1005−1009.
(31) Förster, S.; Timmann, A.; Konrad, M.; Schellbach, C.; Meyer, A.; Funari, S. S.; Mulvaney, P.; Knott, R. *J. Phys. Chem. B* **2005**, *109*, 1347−1360.
(32) Lodge, T. P.; Hamersky, M. W.; Hanley, K. J.; Huang, C.-I. *Macromolecules* **1997**, *30*, 6139−6149.
(33) Hasegawa, H.; Tanaka, H.; Yamasaki, K.; Hashimoto, T. *Macromolecules* **1987**, *20*, 1651−1662.
(34) Bates, F. S.; Fredrickson, G. H. *Annu. Rev. Phys. Chem.* **1990**, *41*, 525.
(35) Corté, L.; Yamauchi, K.; Court, F.; Cloitre, M.; Hashimoto, T.; Leibler, L. *Macromolecules* **2003**, *36*, 7995−7706.
(36) Yu, J. M.; Dubois, Ph.; Jérôme, R. *Macromolecules* **1997**, *30*, 4984−4994.
(37) Abetz, V.; Stadler, R.; Leibler, L. *Polym. Bull. (Berlin)* **1996**, *37*, 135−142.
(38) Russell, T. P.; Hjelm, R. P.; Seeger, P. A. *Macromolecules* **1990**, *23*, 890−893.
(39) Graessley, W. W. *Adv. Polym. Sci.* **1974**, *16*, 48.
(40) Guth, E. *J. Appl. Phys.* **1945**, *16*, 20−25.
(41) Raju, V. R.; Menezes, E. V.; Marin, G.; Graessley, W. W.; Fetters, L. J. *Macromolecules* **1981**, *14*, 1668−1676.
(42) Pakula, T.; Saijo, K.; Kawai, H.; Hashimoto, T. *Macromolecules* **1985**, *18*, 1294−1302.
(43) Honecker, C. C.; Thomas, E. L.; Albalak, R. J.; Hajduk, D. A.; Gruner, S. M.; Capel, M. C. *Macromolecules* **2000**, *33*, 9395−9406.
(44) Daniel, C.; Hamley, I. W.; Mortensen, K. *Polymer* **2000**, *41*, 9239−9247.
(45) Diamant, J.; Williams, M. C.; Soane, D. *Polym. Eng. Sci.* **1988**, *28*, 207−220.
(46) Flozensier, L. S.; Torkelson, J. M. *Macromolecules 25*, 735−742.
(47) Van Krevelen, D. W. *Properties of Polymers*; Elsevier Science B.V.: Amsterdam, 1997.

MA050294E